http://dx.doi.org/10.17159/2411-9717/2015/v115n10a13

The influence of thermomechanical processing on the surface quality of an AISI 436 ferritic stainless steel

by H.J. Uananisa*, C.W. Siyasiya*, W.E. Stumpf* and M.J. Papo†

Synopsis

The need to reduce weight while maintaining good mechanical properties in materials used in the automotive industry has over the years seen an increased exploitation of various steels to meet this new demand. In line with this development, the ferritic stainless steel family has seen a wide application in this industry, with the AISI 436 type increasingly being used for automotive trims and mufflers for exhaust systems, as well as a significant part of this steel's application being for the manufacture of wheel nuts and wheel nut caps in trucks, mainly through the deep drawing process. However, there have been reports of some poor surface roughening of this material during deep drawing, with tearing and/or cracking also reported in some instances. This has been suspected to possibly be associated with some local differences in localized mechanical properties between grains and grain clusters of the rolled and annealed material.

In order to investigate the poor surface roughness exhibited by AISI 436 ferritic stainless steel (FSS) during deep-drawing, Lankford values (R-mean and Δr), grain size, and microtextures of various sheet samples from this steel were studied. The chemical composition range for the samples was 0.013–0.017% C, 17–17.4% Cr, 0.9–1% Mo, and 0.4–0.5% Nb. The steels were subjected to various hot and cold rolling processing routes *i.e.* involving industrial direct rolling (DR) or intermediate annealing rolling (IR), and the drawability and final surface qualities of the steels were compared. It was found that the DR route gave an average R-mean and Δr value of 1.9 and -1.4 respectively, while the IR route yielded an average R-mean and Δr value of 1.6 and 0.52 respectively. The high Δr value for the DR processing route had a substantial adverse effect on the drawability. IR samples exhibited a smoother surface finish on visual inspection, while clear flow lines were visible on the DR samples, despite the fact that DR is the preferred industrial processing route due to the reduced production costs it offers. This observation was also confirmed through SEM examinations. The difference in the surface quality was attributed to microtexture. However, the mechanism responsible for this difference still needs to be identified.

Keywords

ferritic stainless steel, formability, microtexture, EBSD.

Introduction

Owing to the price volatility of nickel over recent years, the need to cut down on the use of nickel in the steelmaking industry has become a matter of keen interest, hence the rising interest in ferritic stainless steels to replace their austenitic counterparts for various industrial applications. Ferritic grades, containing chromium and possibly other stabilizing elements (Ti, Mo, Nb, *etc.*) are well known as cost-saving materials as they do not have the expensive nickel additions (Charles *et al.*, 2008), while at the same time presenting good mechanical properties similar to those offered by austenitic steel grades. Moreover, some standard ferritic grades such as 409, 410, and 430 are readily available all over the world, and are already very successfully used for various applications, such as washing-machine drums and exhaust systems in the automotive industry, and actually have a much broader application potential in many fields (Charles *et al.*, 2008). Since new designs in the automotive industry are driven by safety and environmental concerns, the need to reduce the weight of the exhaust systems while maintaining good resistance to thermal fatigue is continuing to see the exploitation of the ferritic stainless steel family for alternative solutions. Ferritic stainless steels have a relatively low coefficient of thermal expansion and, therefore, some efforts have been made to create new ferritic stainless steels with high yield strengths at elevated temperatures, particularly by the addition of niobium (Nb), which increases the initial high-temperature strength through solid solution hardening (Sello and Stumpf, 2010). The ferritic type AISI 436 is increasingly used for automotive trims, with a major application being for lug nuts or wheel nuts on trucks. It has also seen extensive use in the production of both the central and rear mufflers of exhaust systems, due to its good hot and wet corrosion resistance properties (Charles *et al.*, 2008).

However, during the deep drawing process associated with the manufacture of most of these products, tearing or cracking can sometimes occur. Deep drawing is one of the most common processes for forming metal parts from sheet metal plates, and it is widely used for the mass production of parts in the

* *University of Pretoria, Department of Material Science & Metallurgical Engineering, South Africa.*

† *Advanced Materials Division, Mintek.*

 ISSN 2225-6253. Paper received Aug. 2015.

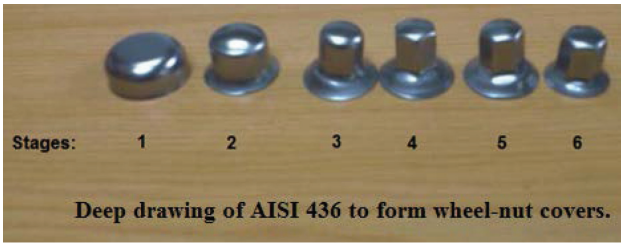

Figure 1 – A multi-stage deep-drawing process for wheel-nut covers

packaging industry, automotive industry, and many others. A typical example of this process is illustrated in Figure 1, which shows some wheel-nut covers manufactured through a six-stage deep-drawing process.

In the reported cases of poor surface roughness, tearing, and cracking, the surface of the drawn products appears to have roughened, possibly due to local differences in mechanical properties between grains or grain clusters of the raw material. This behaviour has been suspected to be a crystallographic texture effect similar to ridging and roping, which is the very common susceptibility of ferritic stainless steel to develop narrow ridges on the sheet surface during forming (Knutsen and Wittridge, 2002; Raabe *et al.*, 2003; Shin *et al.*, 2003). The ridges or undulations result in a very dull surface appearance, which in turn reduces the surface shine and quality of the formed product (Knutsen and Wittridge, 2002). The purpose of this study is to investigate how various thermomechanical processes, with particular emphasis on the processing route, influence this poor surface quality behaviour of AISI 436. This was achieved by studying some crystallographic parameters of the steel, and correlating those parameters to surface topography, in order to help understand the mechanism behind the surface roughening of the steel in subsequent studies. The ultimate objective is to develop possible solutions to the problems experienced in the deep drawing of AISI 436.

Experimental procedure

Various samples of commercial AISI 436 were received and characterized. These were sampled from a production trial operation, as shown in Figure 2, in which two processing routes, direct rolling (DR) and intermediate rolling (IR), were investigated. The emphasis in this study was limited to the final cold-rolled and annealed samples marked F1, F2, F3, and F4 in Figure 2, with thicknesses ranging from 0.46 mm to 0.50 mm.

All the samples were processed from the same 'production heat' and hence had the same chemical composition, shown in Table I.

Each sample was first mechanically polished, etched in an *aqua regia* solution, and examined under an optical microscope to determine the grain structure morphology. Grain-size measurements were determined by the 'Image J' line-intercept method. The samples were then further mechanically prepared to a final fine polish in a colloidal silica medium (OP-S) for electron backscatter diffraction (EBSD) analysis, with the scans being performed using a Jeol JSM-IT300LV scanning electron microscope (SEM).

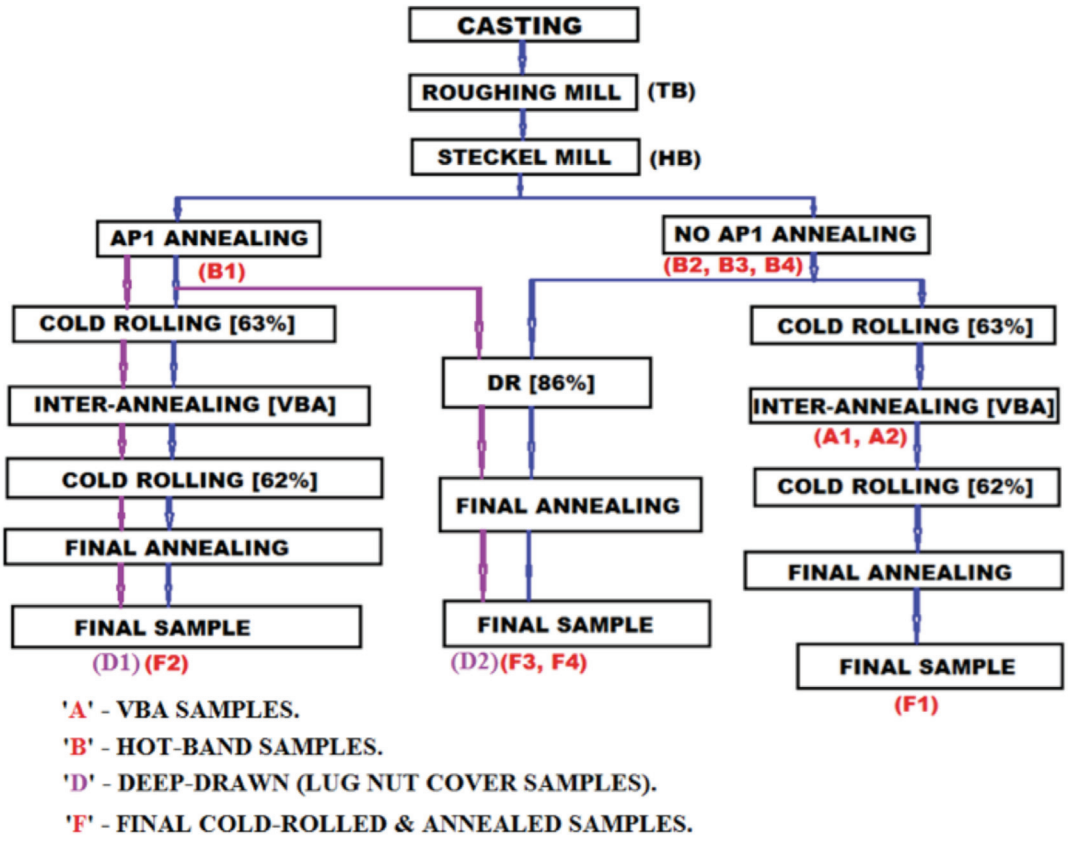

Figure 2 – Block diagram showing the thermomechanical trial processing routes for the AISI 436 samples used in this work

Table I

Chemical composition of the AISI 436, wt.%

C	Mn	Si	P	S	Cr	Mo	Ni	Al	Cu	Nb	Ti	Sn	N
0.013	0.42	0.43	0.022	0.002	17.14	0.94	0.25	0.003	0.09	0.41	0.001	0.012	0.017

Table II

Chemical composition of the deep-drawn AISI 436 samples, wt.%

Sample	C	Mn	Si	P	S	Cr	Mo	Ni	V	Cu	Nb	Ti	Co	N
D1	0.015	0.46	0.55	0.02	0.0005	17.04	0.94	0.15	0.12	0.08	0.50	0.002	0.02	0.02
D2	0.017	0.56	0.38	0.02	0.0005	17.23	0.90	0.24	0.10	0.10	0.37	0.003	0.02	0.02

Orientation distribution functions (ODFs) were further calculated by the series expansion method (l_{max}=22) using the SALSA post-processing software of the CHANNEL5 package. The mean R-values (R_m) and planar anisotropy values (Δr) for the various samples were measured after 10% strain along the longitudinal (0°), transverse (90°), and diagonal (45°) directions. The R_m and Δr values were then calculated using the following standard equations:

$$r_m = \frac{(r_{0^o} + 2r_{45^o} + r_{90^o})}{4} \quad [1]$$

$$\Delta r = \frac{(r_{0^o} + r_{90^o} - 2r_{45^o})}{2} \quad [2]$$

The subscripts 0°, 45°, and 90° refer to the longitudinal, diagonal, and transverse directions with respect to the rolling direction. The planar anisotropy (Δr) gives an indication of the amount of necking or earing that will occur on the edges of the deep-drawn items (Maruma *et al.*, 2013).

Samples of the steel from different production heats, with the compositions shown in Table II, were then deep-drawn into lug-nut covers through the multi-stage forming process shown in Figure 1, and analysed for surface roughness. Sample D1 was intermediate rolled (IR) prior to the deep-drawing process, while D2 was directly rolled (DR). This analysis was used to investigate the effect of the production processing route on the surface roughness of the steel.

Results and discussion

Microstructural analysis

Figure 3 shows the microstructures of the cold-rolled and annealed samples by optical microscopy. Grain size measurements showed an average grain size value of about 25 µm for the four final cold-rolled and annealed samples (F1 to F4), with the respective measured values shown in Table II. It is evident from these results that the processing route

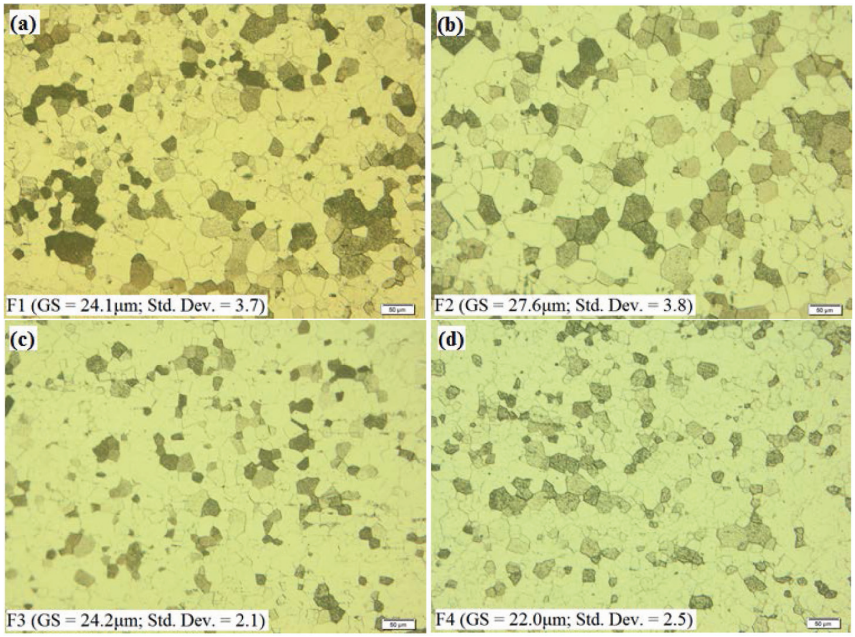

Figure 3 – Microstructures of the samples after a 30-second deep etching in *aqua regia* solution. (a) F1 sample, (b) F2 sample, (c) F3 sample, and (d) F4 sample

Table III

R-mean, Δr, and measured grain sizes

Sample	RHF Dis. temp (°C)	Rolling route	Annealing after Steckel	Rm	delta-r	Grain size (μm)
F1	1079	IR	No	1.55	0.53	24.0 ± 3.7
F2	1083	IR	Yes	1.55	0.51	27.6 ± 3.8
F3	1079	DR	No	1.65	-1.38	24.2 ± 2.1
F4	1160	DR	No	2.07	-1.39	22.0 ± 2.5

had no significant effect on grain size as the average grain sizes measured were within an average ±3 μm standard deviation from each other.

The optical microstructures also clearly reveal various grains that are strongly etched (darker) for all samples, while others are lightly etched. This disparity in grain morphology is caused by differences in grain orientations (Raabe and Lucke, 1992). In order to evaluate the drawability of the sheet samples, measurements of the R-mean (Lankford parameters – R_m) values for each sheet were determined through tensile tests. The results, also shown in Table III, indicated a lower average R_m value for the IR route at about 1.6 compared to an average R_m value of 1.9 for the DR route. It is of particular interest that the planar anisotropy parameter (Δr) for both DR samples is significantly higher in magnitude and negative (average value of -1.4) compared to that of the IR samples (0.52). This behaviour is indicative of a rotation of earing from an angle of 0° and 90° with respect to the rolling direction (RD) to a 45° or 135° direction with respect to RD, which could be attributed to the poor resulting formability of the DR samples despite their higher R_m value.

The severity of the surface roughness of the DR samples was further illustrated by examining one sample from each route by SEM. The micrographs are shown in Figure 4. Both samples were obtained from the 'wall area' of a stage two sample (as shown in Figure 1) from each route, with D1 being from the IR process and D2 from the DR process. It is evident, even by visual inspection of this early forming stage of the two samples, with scans at the same magnification, that the DR sample shows severe surface roughness compared to the flatter surface for the IR sample. Moreover, as may be seen from the distribution of the 'hills and valleys' on the micrographs, some areas on the IR sample seem not to have undergone any deformation (circled regions on 'D1' in Figure 4). This observation calls attention to a phenomenon mentioned by Knutsen and Wittridge (2002), who emphasize the influence of grain size banding in the light of the Hall-Petch effect, hence possible resultant differential yielding under tension. That is to say, clusters consisting of different grain sizes would obviously respond to deformation differently, thereby resulting in distortion of the surface.

Texture evolution

Many studies have shown that ferritic stainless steels, which have a body-centred cubic (bcc) structure, have a tendency to form a preferred orientation of their grains (fibre texture) during rolling and annealing. Siqueira *et al.,* (2011), Huh *et al.,* (2005), and Maruma Siyasiya, and Stumpf (2013) have elaborated on the fact that rolling deformation in most cases leads to a texture characterized by two orientation fibres – an α-fibre texture typically comprising orientations with a common <110> direction parallel to RD (RD//<110>, and a γ-fibre texture comprising orientations of the {111} plane parallel to the RD. Normally, subsequent annealing of cold-rolled sheets increases the γ-fibre component at the expense of the α-fibre, with possible improvements in the formability of the sheet metal (Yazawa *et al.*, 2003). Figure 5 shows the orientation distribution function (ODF) maps of the four samples in this work alongside a Bunge notation texture diagram showing the main texture fibres in bcc taken at Φ=45°. The F1 and F2 IR sample textures are predominantly characterized by a strong γ-fibre, notably {111}<*011*>, {111}<*123*>, and {111}<*112*>, as well as {554}<*225*>. The

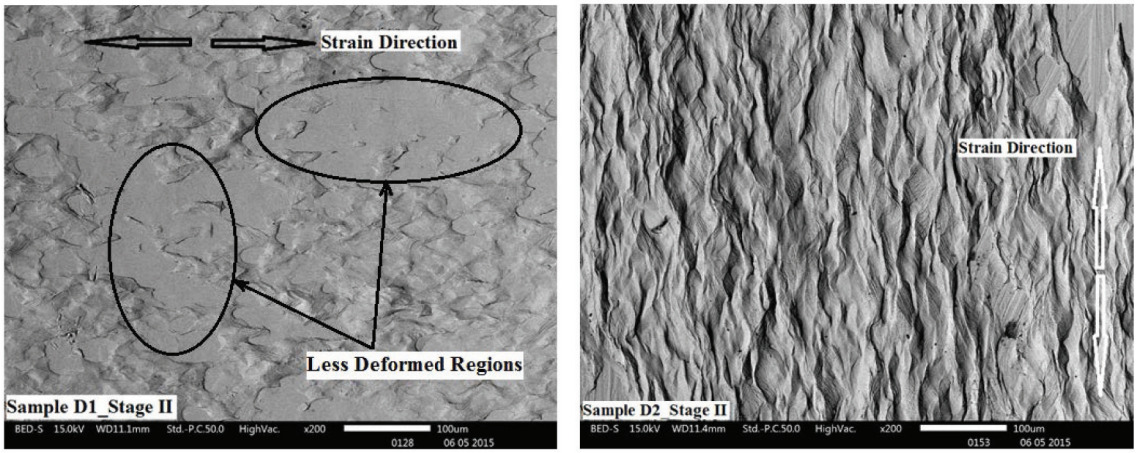

Figure 4 – SEM micrographs of deep-drawn AISI 436 sheets after the second stage of the wheel-nut cover forming process. D1: smoother surface of IR sample, and D2: severe surface roughness of DR sample

striking difference between the two samples is observed in the intensities of these γ-fibres, with the F1 sample showing a stronger intensity of a maximum of about 11 compared to a maximum of about 5 for the F2 sample. This observation clearly illustrates the insignificance of the AP1 annealing process, which is clearly an additional industry cost.

The F3 DR sample, however, is characterized by a strong intensity near or between {322}<258> and {322}<236>. Thus, it is evident that a strong texture component in the {100} plane would always have an adverse influence on the annealing texture (Maruma *et al.*, 2013). This is possibly compounded by the absence of subsequent 'intermediate annealing' in the DR process, which hindered an increase of the γ-fibre evolution. Similarly, the F4 DR sample shows a weak α-fibre near {322}<258> as well as a weak γ-fibre in the vicinity of {554}<225>, despite it having the highest Lankford parameter value (R_m = 2.1). The high negative earing parameter (Δr), which has already been alluded to, is suspected of adversely affecting the formability of these sheets (F3 and F4), despite their good ductility parameters.

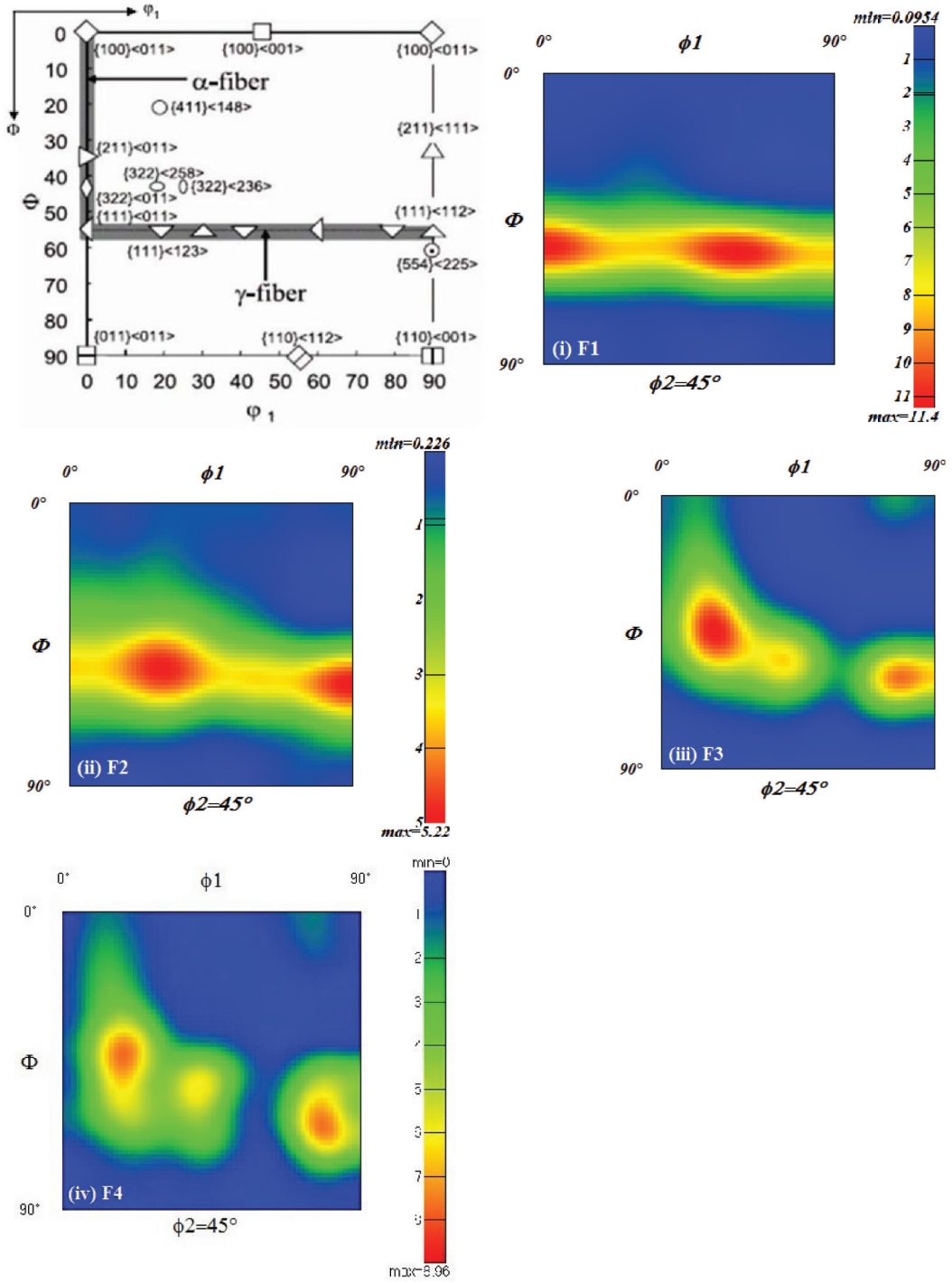

Figure 5 – Orientation distribution function (ODF) maps for the four samples studied. The adjacent diagram shows the texture fibre positions in Euler space (Raabe and Lucke, 1992)

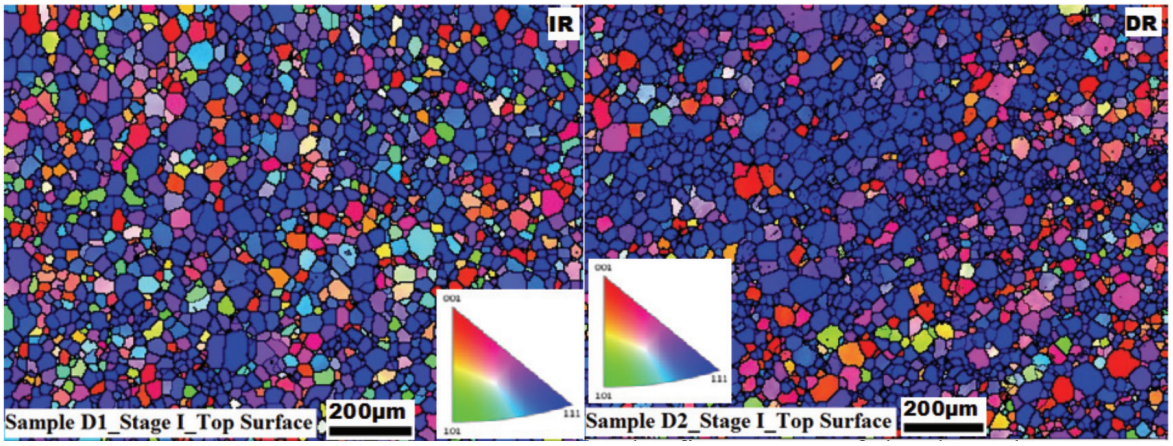

Figure 6 – Inverse pole figure maps //ND for the first stages of the deep-drawn samples, showing clear indications of grain size clustering

Effect of thermomechanical processing on grain size distribution

The grain size clustering effect mentioned above is clearly illustrated by the inverse pole figure (IPF) maps in Figure 6, particularly on the map for sample D2 (the DR sample), in which there is evident clustering of smaller grains separately in a particular region, almost forming a band of smaller grains, and clustering of larger grains in other regions within the microstructures. However, despite this grain size clustering, which may be responsible for differences in yielding across the sheet metal plates and hence the poor surface roughness, no clear texture banding along a particular direction was observed in the microstructures or the SEM images, as is normally the case in ridging and roping. This leads to the conclusion that another localized grain-related mechanism, rather than ridging, is at play in this case.

Conclusions

- Grain size measurements suggested that the processing route had no significant influence on average grain size, but had an effect on grain size distribution
- The intermediate rolling (IR) route resulted in the desired γ-fibre texture, and hence superior surface qualities (surface roughness) in comparison to the direct rolling (DR) route
- In addition, the IR route also resulted in lower planar anisotropy (average $\Delta r = 0.52$) compared to the DR route ($\Delta r = -1.4$), suggesting superior deep-drawability as observed
- Grain-size *clustering* as opposed to texture banding is suspected as a possible factor responsible for surface roughening.

Acknowledgements

The authors gratefully acknowledge the financial contribution provided by the Advanced Metal Initiative (AMI) of the Department of Science and Technology (DST) through the Ferrous Metals Development Network (FMDN), and Columbus Stainless (Middelburg, South Africa). Special thanks are also due to Mr Dave Smith and Mr Jaco Kruger (Columbus Stainless) for their immense contribution and input into this study.

References

Charles, J., Mithieux, J.D., Santacreu, P.O. and Peguet, L. 2008. The ferritic stainless steel family: the appropriate answer to nickel volatility. *6th European Stainless Steel Conference*, Helsinki, 10–13 June 2008.

G. Search, "Euler space - recrystallization textures of metals," [Online]. Available: www.google.com. [Accessed 12 May 2015].

Huh, M.-Y., Lee, J.-H., Park, S.H., Engler, O. and Raabe, D. 2005. Effect of through-thickness macro and micro-texture gradients on ridging of 17% Cr ferritic stainless steel sheet. *Materials Technology - Stainless Steels*, vol. 11, no. 76. pp. 797–806.

Knutsen, R.D. and Wittridge, N.J. 2002. Modelling surface ridging in ferritic stainless steel. *Materials Science and Technology*, vol. 18. pp. 1279–1285.

Maruma, M.G., Siyasiya, C.W. and Stumpf, W.E. 2013. Effect of cold reduction and annealing temperature on texture evolution of AISI 441 ferritic stainless steel. *Journal of the Southern African Institute of Mining and Metallurgy*, vol. 113, no. 2. pp. 115–120.

Raabe, D. and Lucke, K. 1992. Influence of particles on recrystallization textures of ferritic stainless steels. *Steel Research*, vol. 63, no. 10. pp. 457–462.

Raabe, D., Sachtleber, M., Weiland, H., Scheele, G. and Zhao, Z., 2003. Grain-scale micromechanics of polycrystal surfaces during plastic straining. *Acta Materialia*, vol. 51. pp. 1539–1560.

Sello, M.P. and Stumpf, W.E. 2010. Laves phase embrittlement of the ferritic stainless steel type AISI 441. *Materials Science and Engineering Section A*, vol. 527. pp. 5194–5202.

Shin, H.-J., An, J.-K., Park, S.H. and Lee, D.N. 2003. The effect of texture on ridging of ferritic stainless steel. *Acta Materialia*, vol. 51. pp. 4693–4706.

Siqueira, R.P., Sandim, H.R.Z., Oliveira, T.R. and Raabe, D. 2011. Composition and orientation effects on the final recrystallization texture of coarse-grained Nb-containing AISI 430 ferritic stainless steels. *Materials Science and Engineering Section A*, vol. 528, no. 9. pp. 3513–3519.

Yazawa, Y., Ozaki, Y., Kato, Y. and Osamu, F. 2003. Development of ferritic stainless steel sheets with excellent deep drawability by {111} recrystallization texture control. *Society of Automotive Engineers (SAE) of Japan*, vol. 24. pp. 483–488. ◆